INFLUENCE OF PIN SIZE ON TENSILE AND FATIGUE BEHAVIOR OF TI-CFRP HYBRID STRUCTURES PRODUCED BY LASER ADDITIVE MANUFACTURING

Daniel Huelsbusch[1], Matthias Haack[1], Andreas Solbach[2], Claus Emmelmann[2,3] and Frank Walther[1]

[1]Department of Materials Test Engineering, TU Dortmund University
Baroper Straße 303, DE-44227 Dortmund, Germany
Email: daniel.huelsbusch@tu-dortmund.de, web page: http://www.wpt-info.de
Email: matthias.haack@tu-dortmund.de
Email: frank.walther@tu-dortmund.de

[2]Institute of Laser and System Technologies, Hamburg University of Technology
Denickestraße 17, DE-21073 Hamburg, Germany
Email: andreas.solbach@tuhh.de, web page: http://www.tuhh.de/ilas

[3]LZN Laser Zentrum Nord GmbH
Am Schleusengraben 14, DE-21029 Hamburg, Germany
Email: c.emmelmann@lzn-hamburg.de, web page: http://www.lzn-hamburg.de

Keywords: Additive manufacturing, Hybrid structure, CFRP, Damage mechanisms, Fatigue

ABSTRACT

This paper contains mechanical investigations of metallic fabric-penetrating interfaces produced by powder-bed-based laser additive manufacturing and vacuum-assisted resin transfer moulding. Therefore, different fabric penetrations (pins) have been created which vary in length. These penetrative interfaces have been studied in quasi-static tensile (shear) tests and fatigue tests. Deformation and damage processes were determined during tensile and fatigue loading by measurement of the local strain distribution, utilizing a 3D-digital image correlation (DIC) system. Additionally, light microscopic and scanning electron microscopic (SEM) investigations were carried out in order to assess the damage mechanisms and fracture surfaces. The quasi-static tests revealed that tensile shear strength increased by 503 % compared to solely adhesive interface, due to the integration of long pins. Furthermore, different pin-size-depending failure mechanisms have been detected. The fatigue tests showed, that fabric penetration also improves the fatigue strength significantly by 246 %, whereby the damage mechanisms change in comparison to quasi-static failure.

1 INTRODUCTION

Nowadays the increase of energy efficiency is a big challenge in transport industry in order to reduce transportation costs as well as to comply with political requirements. As a consequence, strong efforts are undertaken to optimizing weight in order to reduce fuel consumption. Therefore, lightweight materials with high specific strength such as fibre-reinforced polymers (FRP) have been an essential point of research over the last decades. As a result, high percentages of conventional materials have been substituted by FRPs in serial production such as BMW i3 or Airbus A350 XWB. Even though the usage of FRP is increasing, there is still a need for metallic parts because of their mechanical properties, e.g. isotropic behavior. Thus, multi-material connections and their interface properties became an important part of production and product quality. Two kinds of metal-FRP joining techniques have been industrially accepted: adhesive bonding and mechanical fastening. Unfortunately, adhesive bonding solely generates a joint between the metallic part and the matrix of the FRP. Whereby there is no direct connection between the metal and the actual load-carrying fibres; the strength of the interface exclusively depends on the strength of the adhesive bonding. However, mechanical fastening increases the performance of the interface using form closure and clamping, but it destroys a part of the fibre structure and the clamping forces weaken the FRP. One method of

joining metals and FRP addressing these shortcomings is to create fabric-penetrating interfaces. Ucsnik et al. have carried out initial investigations using an arc welding process to generate pin structures which lead to an increased strength of 11–52 % compared to tensile tests without penetration [1].

Arc welding as well-known manufacturing process has the disadvantage of low accuracy and restricted design parameters. In order to circumvent these disadvantages, Solbach et al. generated penetrative structures using laser additive manufacturing (LAM) to generate complex specimens with near net shape pins [2]. Hereby an essential advantage of the additive manufacturing arises from the high design freedom which allows generating part and pin structure simultaneously. This paper will extend the previous research to estimate the influence of the pin length on tensile shear and fatigue strength as well as the accompanying failure-initiating mechanisms.

2 EXPERIMENTAL PROCEDURES

2.1 Additive manufacturing of test specimen

The metallic parts of the specimens used for the quasi-static and cyclic investigations were manufactured on a single LAM machine with identical process parameters. Frequent machine maintenance and laser power measurements ensure the process reproducibility across the different manufacturing batches. The machine is a commercially available LAM system with a 200 W laser (EOS, Type EOSINT M270 XT). For the additive manufacturing of the specimens a layer thickness of 30 µm and an energy density E of 45.3 J/mm³ were used. The melting process took place in inert atmosphere using an argon-floated building chamber. Hereby the parts are generated by melting Ti-6Al-4V powder layerwise with a laser beam (Fig. 1). The specimens were built with an orientation of 45° to the build platform to create a surface with a specific roughness on the plate and the pins.

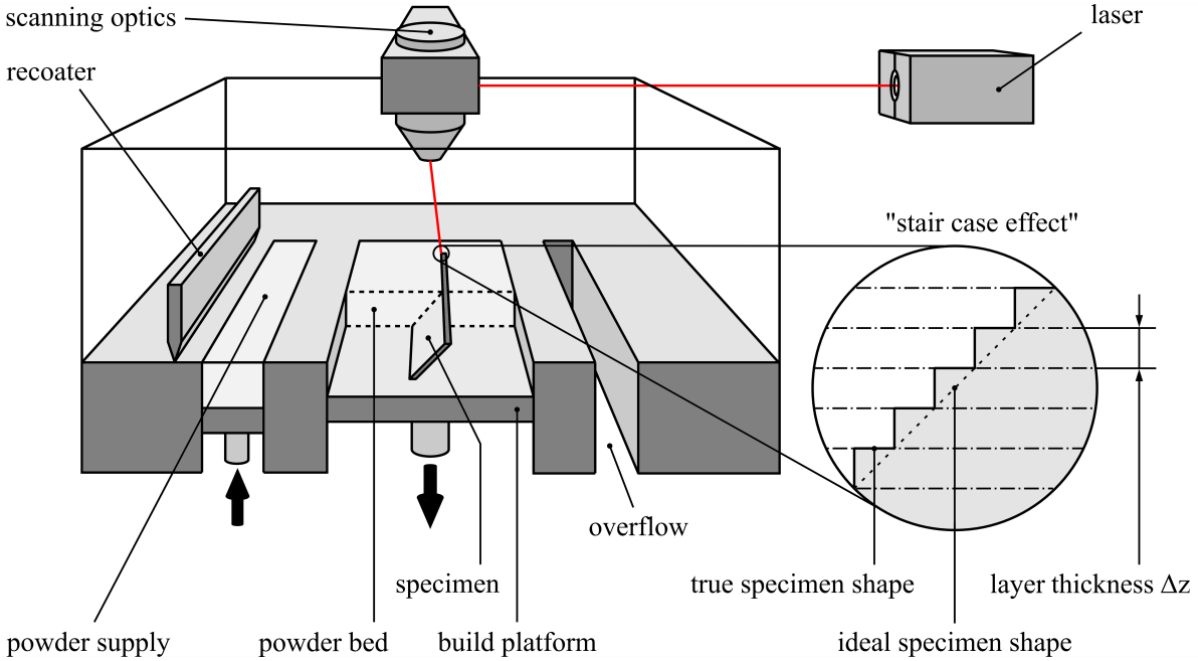

Figure 1: Principle of laser additive manufacturing.

For relaxation of residual stresses induced by local heating and fast cooling, a post-process heat-treatment for 3h at 650°C in argon with subsequent argon cooling was performed. Wire erosion was used to cut the specimens from the base plate and an abrasive as well as a shot blasting was used to optimize surface roughness.

For the multi-material structures a non-symmetric geometry for the single shear lap specimens has been designed in accordance to DIN EN 1465:2009-07 (Fig. 2). To analyse the influence of

penetrative structures, the length of the pins was varied. Therefore, three different specimen types with pin lengths of 2.0 mm and 0.5 mm as well as a reference without pins were built.

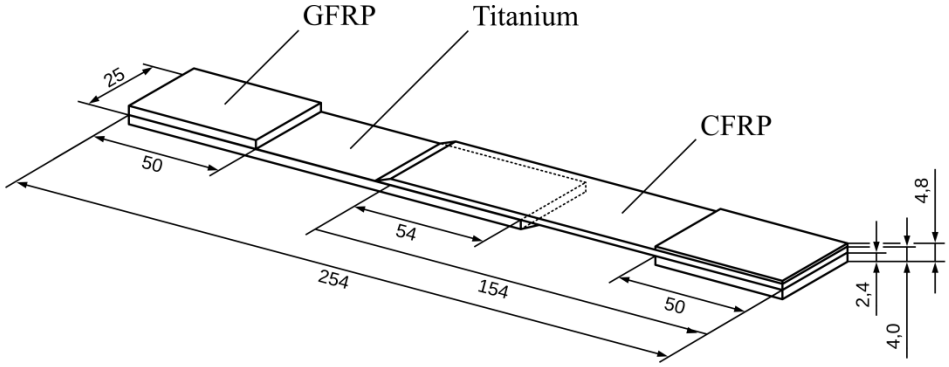

Figure 2: Design of Ti-CFRP hybrid specimens.

To complete the manufacturing of the specimens, dry twill weave carbon fibre was laid onto the metallic substrate. The pins were pushed through the fabric with low forces and without further devices to generate a positive-locking interface. Subsequently, vacuum-assisted resin transfer moulding (VARTM) was used to infuse epoxy resin through the dry fibre fabric (co-bonding). Curing took place at room temperature without post-heating.

Exemplary microscopic pictures of the saturated interface are given in Figure 3 for both pin sizes. As shown in Figure 3a, the 0.5 mm long pin penetrates the first fibre layer. Additional layers could not be fully penetrated. In comparison, 2.0 mm pins pierce through nearly every layer of the carbon fibre reinforced polymer (CFRP) (Fig. 3c). Both pin lengths penetrate the fibre bundles of the twill fabric without destruction. The fibre bundles open themselves in case of penetration and create an accumulation of resin before and after the pin in fibre orientation during the VARTM process (Fig. 3b and 3d).

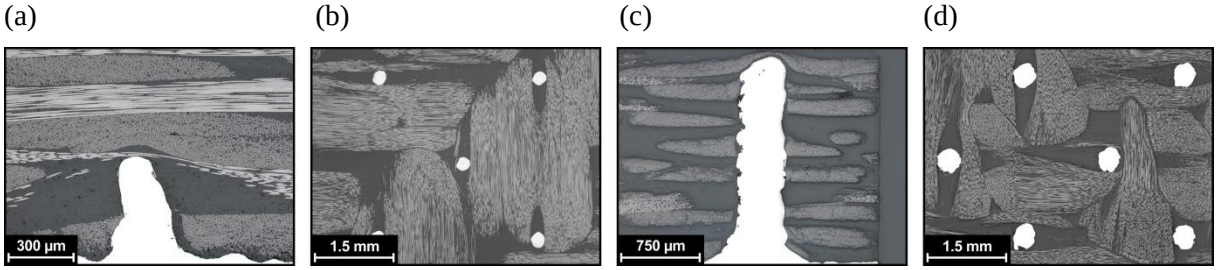

Figure 3: Specimens with (a-b) 0.5 mm pins and (c-d) 2.0 mm pins, cut in axial and orthogonal direction.

2.2 Quasi-static investigations

Quasi-static tensile tests were performed to assess the influence of the pin length on the tensile shear strength and the corresponding damage mechanisms. The tests were carried out at universal testing system (Shimadzu, Type AG-X, $F_{max,stat}$ = 100 kN). The test parameters were defined in accordance to DIN EN 1465:2009-07. The tests were performed force-controlled with $\dot{F}$ = 100 N/s until specimens failure at an abort criterion defined as a drop of 5 % of maximum force. Each test was carried out at 20°C and 40 % relative humidity. A linear variable differential transformer (LVDT) was used for elongation measurements. Furthermore, strain measurements were performed using 3D-digital image correlation (DIC) (Limess, Type Q400), to determine the local strain at the surface depending on the stress to identify the corresponding damage mechanisms.

2.3 Fatigue investigations

For the estimation of relation between pin length and fatigue properties, multiple step tests (MST) [3] were performed on a servo-hydraulic testing system (Schenck/Instron, Type PC63M, F_{max} = ± 50 kN) with a stress ratio of R = 0.1 and a frequency of 5 Hz using sinusoidal load-time functions. MSTs have already been used successfully for resource-efficient estimation of the fatigue behavior of CFRP and additive manufactured metallic parts [4, 5]. Figure 4a shows the principle of the MST. Starting at $F_{max,start}$ = 500 N, the maximum force was increased stepwisely by ΔF_{max} = 500 N after step lengths (ΔN) of 10,000 cycles until fracture at an abort criterion of ± 4 mm displacement. The tests were performed at 20°C and 40 % relative humidity. As a material response, the displacement amplitude s_a was recorded in order to assess the fatigue performance. Therefore the change of displacement amplitude per step was used to detect the damage initiation as well as to describe the progress of damage until specimens failure (Fig. 4b).

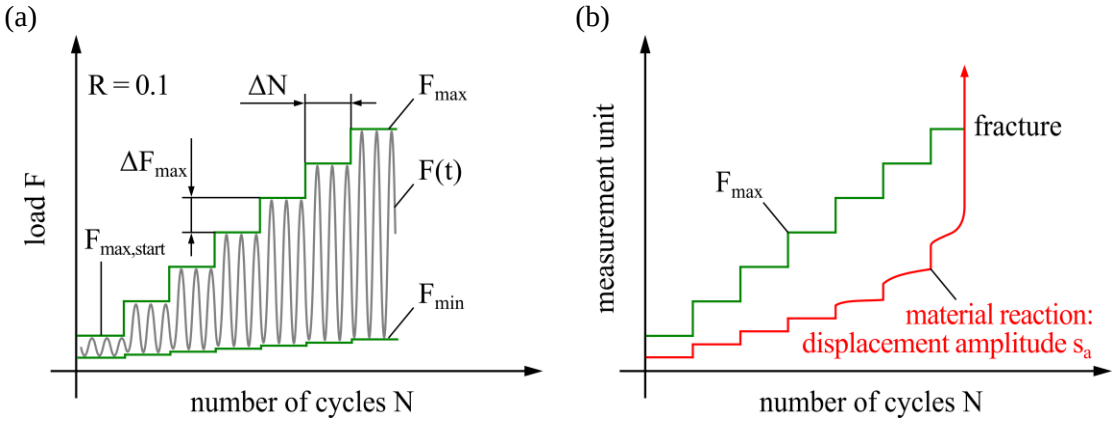

Figure 4: a) Scheme of multiple step test, b) development of material response in multiple step test.

2.4 Microstructural investigations

Microstructural investigations were carried out to analyze the initial state of the hybrid structures and the fracture surface for determination of damage mechanisms. Therefore light microscopic (LM) (Zeiss, Type Axio Imager M1m) and scanning electron microscopic (SEM) (Tescan, Type Mira3 XMU) investigations were performed. A standardized pre-treatment process was specified: The specimens were cut into segments which were embedded in a cold-mounting-process using Struers Epofix epoxy resin; the parts were manually grounded and finally polished using a water-based (3 µm) diamond suspension on an artificial silk woven disk. For SEM investigations a gold coating was sputtered onto the segments surface.

3 QUASI-STATIC RESULTS

3.1 Tensile tests

The results of the quasi-static tensile tests for the different pin lengths are illustrated in Figure 5. In Figure 5a the load F is displayed as a function of elongation Δl for each pin length. At the beginning, each graph shows a nearly identical linear slope. Between 0.25 mm and 0.75 mm of elongation, the curves present a turning point: The apparent stiffness decreases and the curves change from approximately linear to progressive increase. For the bonded specimens, this behavior isn´t particularly extensive; the gradient decreases after the turning point until fracture. For each specimen the failure occurred abruptly without any previous degradation of the mechanical properties. However, acoustic signals have been detected in an early stage, which indicate fibre-breaking or crack-initiation of the adhesive interface due to overloading. Each pin length leads to specific damage profiles which will be investigated in chapter 3.2. Every specimen shows instantaneous and complete fracture. In Figure 5b the fracture load P is displayed for the corresponding pin length to visualize the influence of form-closed joining via additive manufacturing on the shear strength. For each pin length the

arithmetic average of fracture load P has been calculated in accordance to DIN EN 1465:2009-07 and illustrated in the bar chart (Fig. 5b) with accompanying standard deviation s_n.

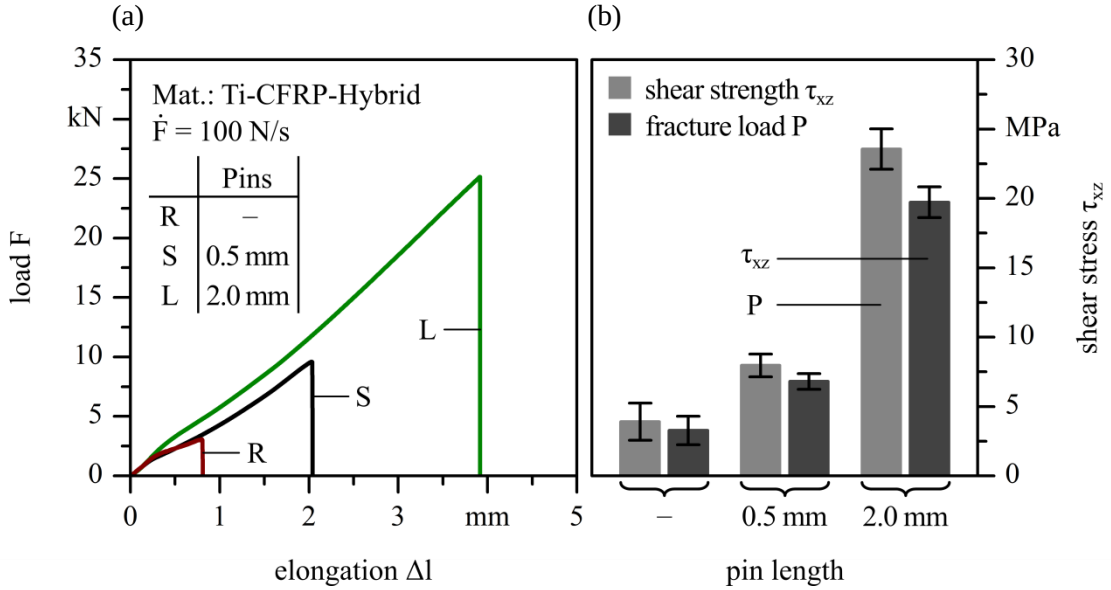

Figure 5: a) Load-elongation diagrams, b) shear strengths and fracture loads in dependence of pin length.

Furthermore, the shear strength τ_{xz} has been determined with respect to the joining surface A (Eq. 1), in order to address little deviations of A due to partly manual manufacturing of the specimens. The additional parameter τ_{xz} considers this variation and offers a greater comparability.

$$\tau_{xz} = \frac{P}{A} \tag{1}$$

The quasi-static results are plotted in Table 1. The average shear strength τ_{xz} = 19.73 MPa of the specimens with long pins represents an increase of 503 % compared to the reference specimens (τ_{xz} = 3.27 MPa). A pin length of 0.5 mm leads to an increment of about 108 % (τ_{xz} = 6.80 MPa). Comparing the values of the coefficient of variation v, the reference specimens show a large spread: the standard deviation s_n of shear strength is equivalent to one third of the arithmetic average. The pin-reinforced structures exhibit more consistent material behavior. Comparable series of tests carried out by Smith and Kellar [6] and Parkes et al. [7] resulted in shear strength of 7.80 MPa resp. 11.40 MPa for solely adhesively bonded Ti-CFRP single lap specimens. These values indicate a great potential for optimizing the adhesive interface discussed in this paper. However, the results demonstrate that including form-closed joining by pins (via additive manufacturing) in bonded hybrid structures improves the shear strength significantly and leads to more reproducible material properties.

Parameter		Pin length –	Pin length 0.5 mm	Pin length 2.0 mm
Fracture load P	[kN]	4.55	9.28	27.48
Standard deviation s_n	[kN]	1.57	0.96	1.70
Coefficient of variation v	–	0.35	0.10	0.06
Shear strength τ_{xz}	[MPa]	3.27	6.80	19.73
Standard deviation s_n	[MPa]	1.03	0.56	1.11
Coefficient of variation v	–	0.32	0.08	0.06

Table 1: Fracture load and shear strength values in dependence of pin length.

3.2 Fracture analysis

In quasi-static tensile tests, each pin length leads to a different, completely reproducible failure characteristic. The reference specimens without pins exhibit completely adhesive failure on the titanium side. The specimens with a pin length of 0.5 mm also fail in the joining zone. SEM-analysis confirmed a combination of adhesive and cohesive failure. The fracture surface exhibits an adhesive failure on the titanium side. However, the pins at the joining edge remained completely intact (Fig. 6a), whereas the pins located at the opposite end sheared just a few microns above the surface (Fig. 6b). At the intact pins residues of CFRP were detected in loading direction. This suggests that a cleavage occurs due to a relative movement of the titanium and CFRP which leads to partly cohesive failure.

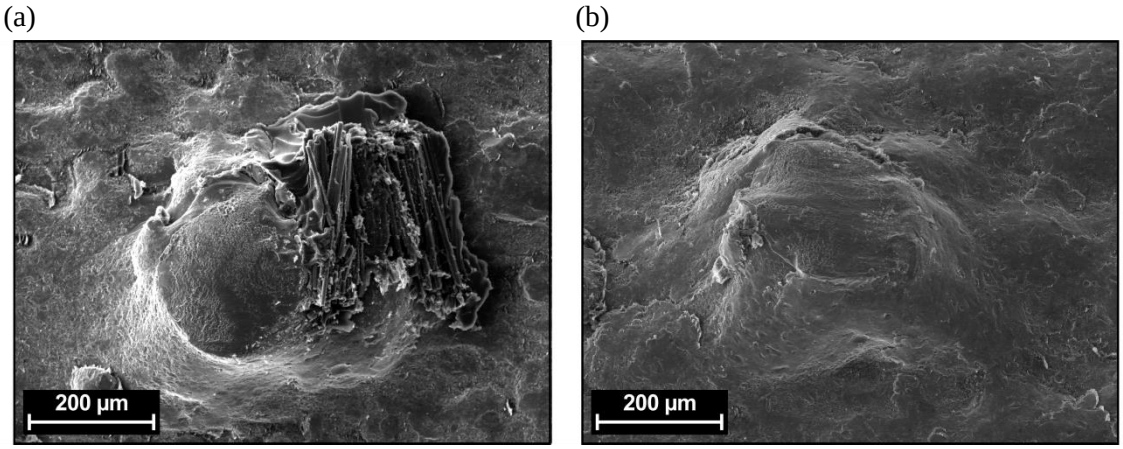

Figure 6: (a-b) Fracture surface analysis of specimens with pin length 0.5 mm.

The specimens with a pin length of 2.0 mm show a net tension failure of the CFRP-structure at the first row of pins (Fig. 7). The detected fracture complies to a translaminar crack propagation in plane of axial normal stress σ_{xx}. A cohesive failure of the polymer matrix at the joining edge and pins occurred. This behavior includes a partly adhesive failure of the interface. The CFRP shows typical fibre pull-out in loading direction. The warp fibres present intralaminal decohesion. The pins itself do not show any plastic deformation. It appears that the failure can be characterized exclusively by cohesive fracture of the CFRP.

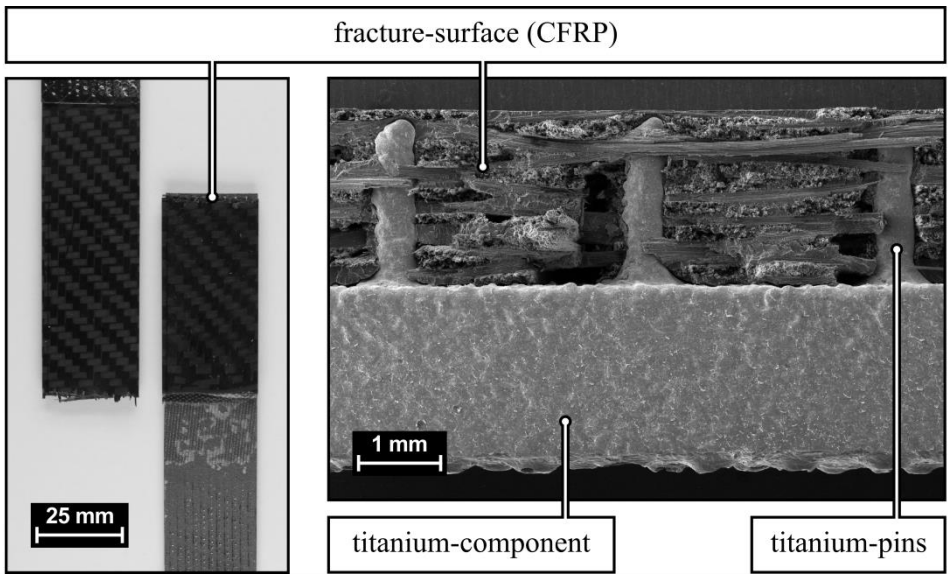

Figure 7: Fracture surface analysis of specimens with pin length 2.0 mm.

3.3 Local strain analysis

The titanium and CFRP components can be described as flat parts with little extension in z-axis. Due to this geometry, it can be assumed that relevant damage processes lead to inhomogeneous deformation which can be detected at the surface. The DIC-system allows to visualize the deformation state with temporal and spatial resolution. The DIC has been supplemented by video recordings of the specimens narrow edge.

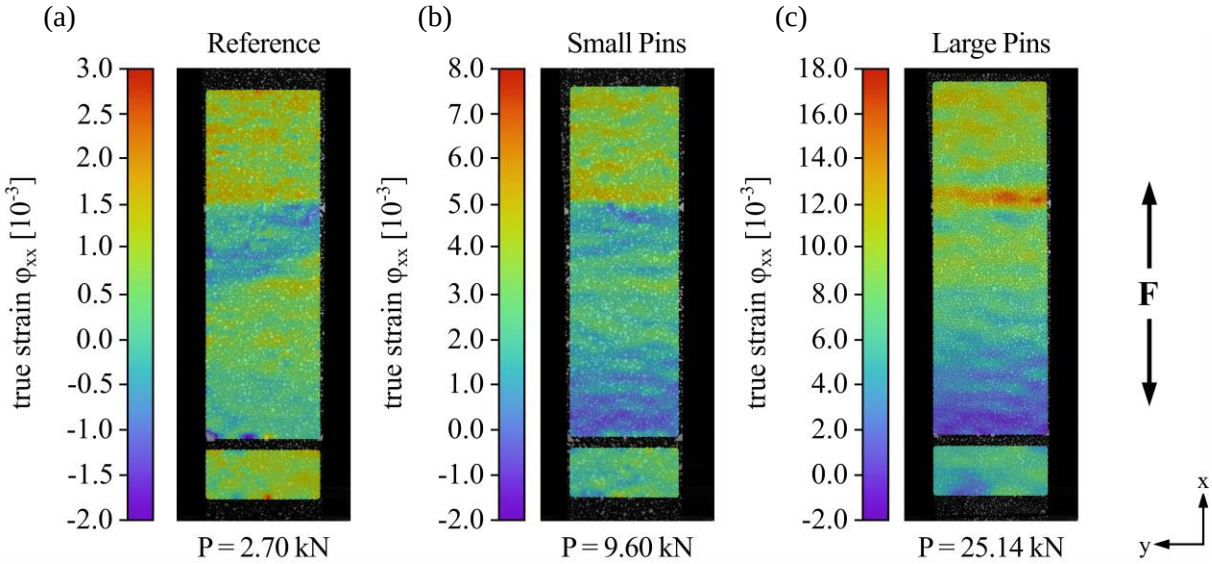

Figure 8: DIC-analysis for each pin length at fracture load.

In Figure 8 the deformation state for each pin length is compared by their local true strain φ_{xx} at their specific fracture load P. It is conspicuous, that the maximum true strain φ_{xx} differs significantly between each pin length. Furthermore, the distribution of local strain on the surface of the reference specimens and the specimens with 0.5 mm pins is similar with respect to the scaling. Contrary results are perceived for the specimens with 2.0 mm pins which exhibit local strain concentration at the joining edge as well as an overall different distribution of surface strain.

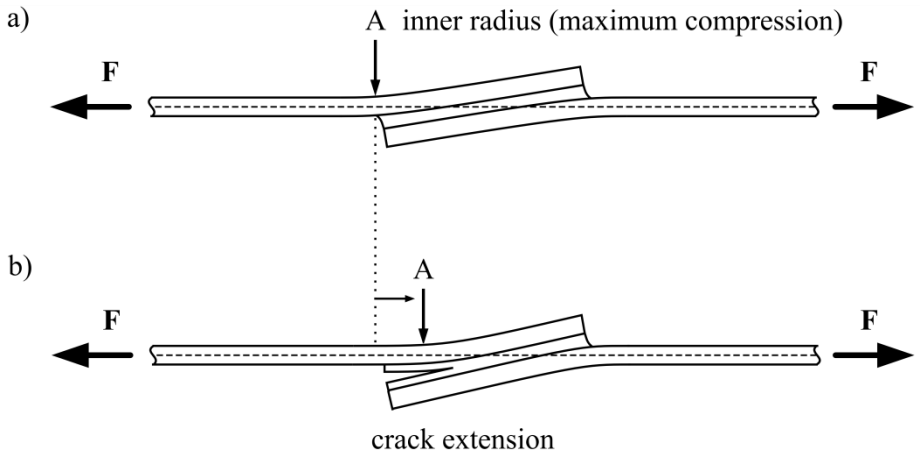

Figure 9: Deformation behavior of adhesively bonded single lap joints [8, 9].

The local strain conditions for each specimen can be explained more differentially considering the macroscopic deformation caused by the specimens design and loading direction. Due to the asymmetric layout, a bending moment M_B occurs in single lap joints. This leads to a deformation of the components, because the specimen forces an overlap of its middle axis with the pitch line of load

(Fig. 9a). In this scenario a high local peel stress develops at the joining edge which results in debonding due to the low tensile strength of the interface (Fig. 9b) [8].

With respect to the macroscopic deformation process, the local strain distribution of the reference specimens (Fig. 8a) can be discussed. The indicated negative local strain is the result of a surface compression due to the bending moment (Fig. 8a and 9). This corresponds to an increase of peel stress which leads to a beginning of adhesive failure of the interface. The crack propagation is governed by increasing load F. Immediately before fracture at F = 2.70 kN, the affected area reaches its maximum. A less minimum true strain of $-0.5 \cdot 10^{-3}$ (Fig. 8a) in comparison to the condition at F = 2.03 kN ($\varphi_{xx,min} = -1.25 \cdot 10^{-3}$) can be detected. This is due to a superimposed tensile stress and a decreased bending moment because of a new-orientation of the titanium and CFRP components which represents a complex three-dimensional deformation state. The structure fails completely adhesively at the titanium side (Chap. 3.2).

The damage process of the specimens with 0.5 mm pins is qualitatively similar to the reference specimen, even though the quantitative values for the true strain and shear stress are increased. Figure 8b illustrates that the true strain φ_{xx} achieves a maximum of $5 \cdot 10^{-3}$ on the surface of the CFRP component, whereas the average true strain φ_{xx} on the overlap area is about $1 \cdot 10^{-3}$. The failure occurs at the interface comparable to the reference specimens, yet different damage mechanisms can be detected (Chap. 3.2). The increasing bending moment induces a greater macroscopic deformation of the components which leads to a pull-out-effect in the area of the joining edge. The damaged area is extended with increased loading until the remaining pins fail cohesively which could be verified by camera recording (Fig. 6b).

The behavior of the specimens with large pins is contrary to the above described damage processes. In Figure 8c a local strain concentration is displayed at the joining edge. Because of the linear elastic behavior of CFRP, the inhomogeneous deformation is likely due to an increase of stress at the joining edge. A load F of 25.14 kN complies to a maximum true strain of $16 \cdot 10^{-3}$ (F = 12.57 kN → $\varphi_{xx,max} = 7 \cdot 10^{-3}$) which leads to a net tension failure of the CFRP. Despite the bending moment induces a deformation, camera recordings show that the large pins remain embedded in the CFRP component until fracture.

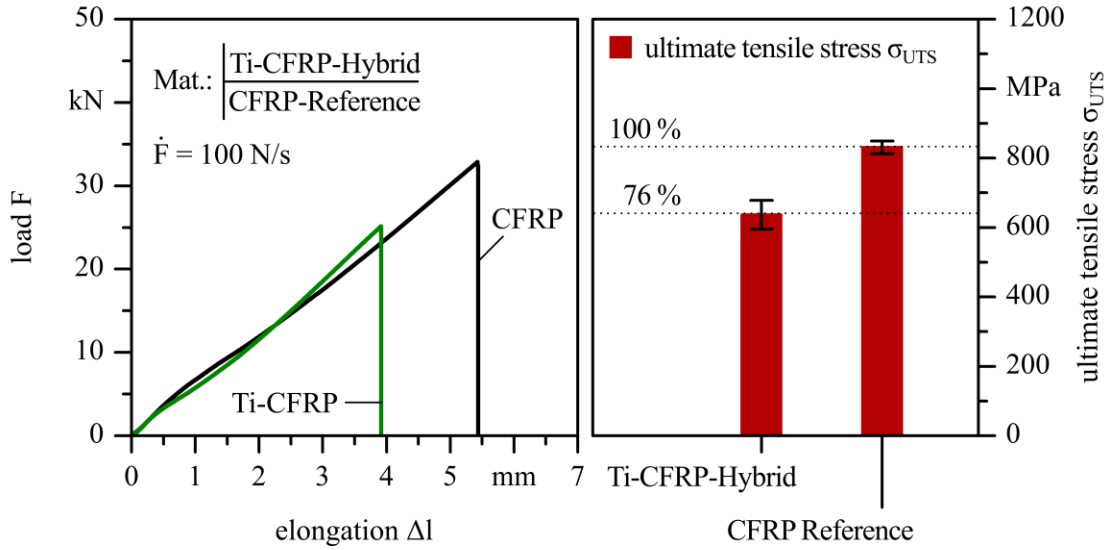

Figure 10: Tensile strength of Ti-CFRP with pin length 2.0 mm and monolithic CFRP.

It can be concluded that applying pins via additive manufacturing in hybrid structures causes a positive influence on the shear strength. Furthermore, it is evident that an enlargement of the pin length up to the CFRP-thickness increases the shear strength significantly. This is due to a permanent mechanical interlocking, although the loading leads to a deformation and an adhesive failure of the interface. Consequently a high local strain at the joining edge arises which results in net tension failure

of the CFRP. Because of this failure behavior, the calculated shear strength τ_{xz}^{*} = 19.73 MPa is to be considered a virtual value which is less than the real shear strength τ_{xz}. A comparison of the ultimate tensile strength σ_{UTS} for the CFRP in the hybrid structures and monolithic CFRP-specimens shows that the inclusion of fabric-penetrating pins leads to a decrease of about 24 % in tensile strength (Fig. 10). The geometry as well as the distribution of the pins have to be optimized in order to achieve a more homogenous strain distribution at the joining edge and joining surface, leading to an increase in tensile and shear strength.

4 FATIGUE RESULTS

4.1 Multiple step tests

The displacement amplitude s_a was used as basis for assessment. Excluding any pre-damages of the components, a linear relationship between maximum load F and displacement amplitude s_a can be assumed in correspondence to the quasi-static behavior. Thus, a change of the load-displacement relationship is regarded as an indicator for damage progression at the primary stressed interface. In order to discuss the material response, a relative change in displacement amplitude $\Delta s_{a,rel}$ was calculated which portraits the percentage change of displacement amplitude per step.

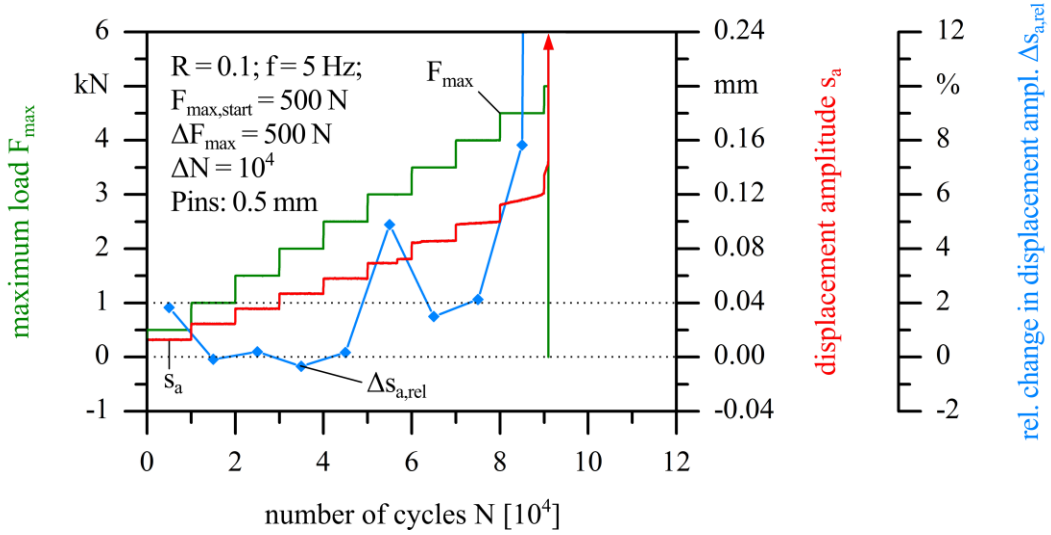

Figure 11: Multiple step test for a specimen with 0.5 mm pins.

In Figure 11 the result of a multiple step test (MST) is exemplarily shown for a specimen with 0.5 mm pins. At a maximum load F_{max} = 3.0 kN a discrete change of the displacement amplitude s_a is detected which corresponds to a relative change in displacement amplitude $\Delta s_{a,rel}$ of about 5 %, followed by a progressive degradation of the mechanical properties. It is likely, that the sudden increase of s_a illustrates a brittle damage occurrence which leads to an evolving damaging process. Subsequently, the values of s_a and F_{max} do not have a linear relationship which can be derived from the curve shape of $\Delta s_{a,rel}$ (Fig. 11). It can be assumed, that this process corresponds to a debonding of the adhesive fillet at the joining edge, followed by crack growth in the interface until failure at a maximum load of 5.0 kN.

The MSTs for each pin length result in a quantitatively similar curve shape concerning the progress of the displacement amplitude s_a; in every MST a similar event, leading to a sudden change of s_a can be detected. However, the values for the maximum load F_{max} and the number of cycles N vary specifically for each pin length. The results for the MSTs are displayed in Figure 12. The maximum load at failure (strength $F_{max,f}$) and the maximum load at first damage occurrence (threshold $F_{max,d}$) are visualized for each test.

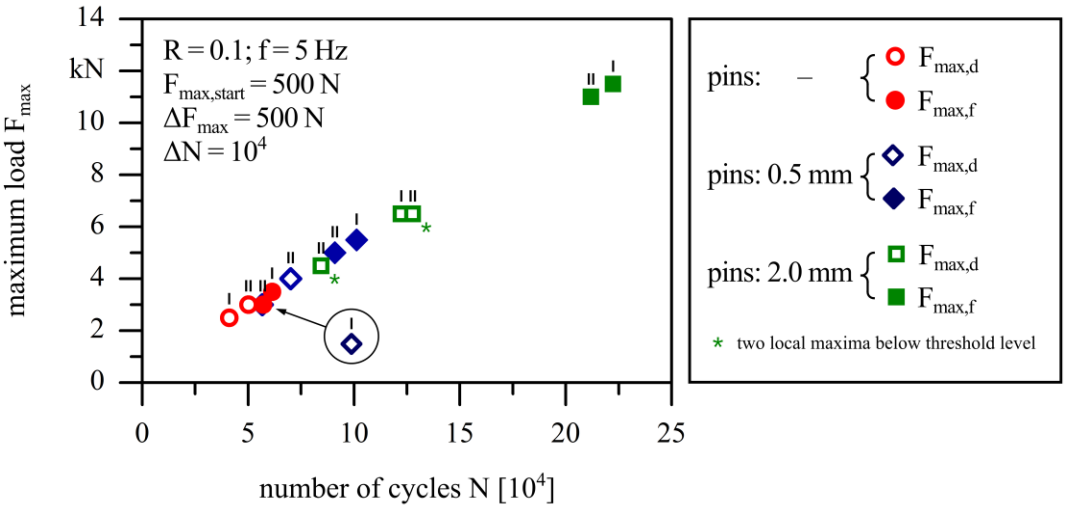

Figure 12: Maximum loads at failure and first damage occurrence determined in multiple step test for different pin lengths.

It is evident, that in comparison to the reference specimens the specimens with 2.0 mm pins lead to an increase of number of cycles to failure by 267 % to $N_f = 21.7 \cdot 10^4$ corresponding to an enhancement of strength of about 246 % to $F_{max,f}$ = 11.25 kN. Furthermore, the number of cycles to first damage are doubled ($N_d = 10.3 \cdot 10^4$). The 0.5 mm pins offer less potential. The strength is increased by 62 % ($F_{max,f}$ = 5.25 kN) in comparison to the adhesively joined specimens, whereas the threshold $F_{max,d}$ is enlarged by just 39 %. The results show a significant improvement of the fatigue behavior of the additive-manufactured specimen due to an integration of large pins. Though the first damage process can be detected by the change of displacement amplitude at an early stage of $F_{max,d}$ = 5.50 kN, the structure and interface do not seem to show a relevant and critical damage state. The number of cycles as well as the maximum load can be more than doubled until failure. This represents a slow and continuous damage process in comparison to the quasi-static behavior. However, the relative improvement of fatigue strength (246 %) is less than the relative increase of shear strength (min. 503 %) by implementation of pins. In order to determine the reason for the different influence of varied pin sizes, fracture analyses were carried out.

4.2 Fracture analysis

Each specimen configuration is associated with a distinctive damage pattern. Under fatigue loading the polymeric part of the hybrid specimen is not the primary source of failure, except the reference specimens which failed adhesively.

Fracture analysis showed, that approximately one half of 0.5 mm long pins failed due to fatigue and/or shear stresses, the other half remained intact. Unlike the previously mentioned cluster of intact pins at the joining edge, whole pins can now be detected all over the joining area, frequently surrounded by their fractured counterparts. Although there are some domains where one of the two pin-conditions prevails, there is no clear pattern which could be tied to a specific development of damage. One example of the two kinds of pin conditions is shown in Figure 13a. In case of pin fracture, the upper fragment usually remains embedded in the CFRP matrix. The fracture surface has a multi-facetted structure which is an indicator of inter-granular crack-propagation. One example is depicted in Figure 13 b. The dark covering visible in the lower left part has been confirmed to be part of the polymeric matrix.

In case of 2.0 mm pins, a complete rupture of all elements occurred at a high loading level. Two distinguishable shapes of fracture surfaces exist. Next to the joining edge, the pins fail above the pin-root and the fracture surfaces resemble the ones of the specimen with smaller pins. Apparently the failure of the first rows of pins involves a change in loading state, because in the next few rows, the fatigue crack originates at the pin root but propagates into the metallic substrate, so more material is

removed from the surface in case of a global failure which leads to the formation of crater-like immersions (Fig. 14 a). A similar behavior has been documented by Parkes et al. [9], who attribute the different modes of crack propagation to a change in the grade of macroscopic specimen deformation.

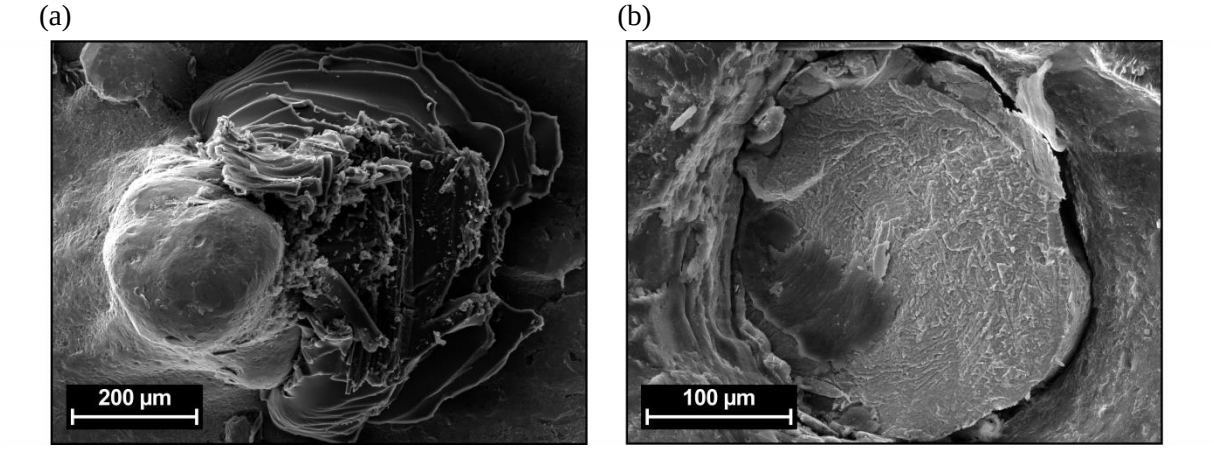

Figure 13 (a–b) Fracture surface analysis of specimens with pin length 0.5 mm.

In Figure 14a the fatigue crack originated at a penny-shaped crack, visible at the lower right side. Most of the other pins did not depict such a recognizable path of crack propagation. Although the fatigue behavior of the investigated specimen is primarily governed by the metallic part, whose strength to withstand cyclic loading is apparently lower than its CFRP-counterpart which in consequence confirms the first evidence of fatigue damage in the matrix polymer. As depicted in Figure 14b, smaller parts in the CFRP-structure are missing which are located at the surface of the corresponding titanium part. This type of delamination is the first form of cohesive failure documented for this polymer system, besides the net-tension failure in the quasi-static investigations.

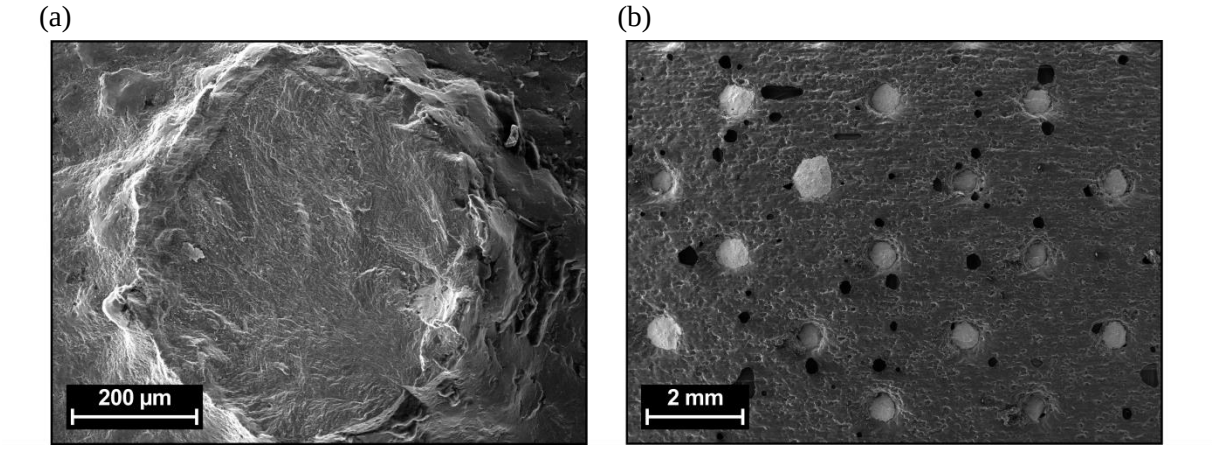

Figure 14 (a–b) Fracture surface analysis of specimens with pin length 2.0 mm.

5 CONCLUSIONS

Laser additive manufacturing (LAM) offers a great potential to optimizing the strength of the interface of hybrid structures. By LAM, pin structures were applied on the surface of the Ti-component which penetrated the fiber-reinforced polymer and implemented an additional form closure within the fabric. Quasi-static tensile tests show that insertion of 2.0 mm pins in the hybrid structure leads to an increase of shear strength by min. 503 % in comparison to a solely adhesively joined structure. Furthermore more reproducible material properties are achieved, represented by a reduced value of the coefficient of variation. Microstructural investigations have shown that different pin lengths induce diverse, partly complex damage mechanisms. The 0.5 mm pins lead to mostly adhesive failure accompanied by additional local cohesive damage of the CFRP and partly sheared off metallic

pins. Long pins result in a net-tension failure of the CFRP instead. Fatigue tests confirm the potential of penetrated structures for optimizing the mechanical properties. The maximum load to failure was increased by 246 % due to the inclusion of 2.0 mm pins in comparison to the reference specimens. Furthermore, fatigue loading leads to a change in damage process compared to the quasi-static behavior. A cohesive failure occurred, represented by sheared off pins, as a consequence of less pronounced fatigue strength of titanium as against CFRP. As a result, the fatigue strength of the hybrid structures has been less increased by the integration of pins (246 %), than the quasi-static shear strength (503 %).

In further investigations, the pin geometry, number of pins and their allocation will be optimized in order to generate a homogenous distribution of strain in quasi-static tensile tests, leading to an improved damage behavior and an increase in shear strength. In addition the pin geometry will be fitted to the macroscopic deformation of the single lap specimen by generating an undercut to prevent the debonding of the Ti- and CFRP-components. In this context, due to the complex relationships between quasi-static and fatigue behavior, it has to be ensured, that the fatigue properties will not be deteriorated by an altered pin geometry and allocation for quasi-static mechanical properties.

REFERENCES

[1] S. Ucsnik, M. Scheerer, S. Zarenba and D.H. Pahr, Experimental investigation of a novel hybrid metal-composite joining technology, *Composites: Part A*, **41**, 2010, pp. 369-374 (doi: 10.1016/j.compositesa.2009.11.003).

[2] A. Solbach, D. Huelsbusch, M. Haack, C. Emmelmann and F. Walther, Investigation of fiber reinforced plastic penetration produced by laser additive manufacturing with pin size variation, *Proceedings of the 5th International Workshop on Aircraft System Technologies, Hamburg, Germany, February 25-25, 2015*, pp. 315-323 (ISBN 978-3-84403319-9).

[3] F. Walther, Microstructure-oriented fatigue assessment of construction materials and joints using short-time load increase procedure, *MP Materials Testing*, **56**, 7-8, 2014, pp. 519-527 (doi: 10.3139/120.110592).

[4] D. Huelsbusch and F. Walther, Damage detection and fatigue strength estimation of carbon fibre reinforced polymers (CFRP) using combined electrical and high-frequency impulse measurements, *Proceedings of the 6th International Symposium on NDT in Aerospace, Madrid, Spain, November 12-14, 2014, The e-Journal of Nondestructive Testing*, **20**, 1, pp. 1-9 (ISSN 1435-4934).

[5] S. Siddique, M. Imran, E. Wycsik, C. Emmelmann and F. Walther, Influence of process-induced microstructure and imperfections on mechanical properties of AlSi12 processed by selective laser melting, *Journal of Materials Processing Technology*, **221**, 2015, pp. 205-213 (doi: 10.1016/j.matprotec.2015.02.023).

[6] F. Smith and E. Kellar, Energy absorbing joints between fibre reinforced plastics and metals, *Proceedings of the International Conference Joining Plastics, London, UK, April 25-26, 2006*, pp. 1-10.

[7] P.N. Parkes, R. Butler and D.P. Almond, Static strength of metal-composite joints with penetrative reinforcement, *Composite Structures*, **118**, 2014, pp. 250-256 (doi: 10.1016/j.compstruct.2014.07.019).

[8] M. Imanaka, K. Haraga and T. Nishikawa, Fatigue Strength of Adhesive/Rivet Combined Lap Joints, *The Journal of Adhesion*, **49**, 3-4, 1995, pp. 197-209 (doi: 10.1080/00218469508014356).

[9] P.N. Parkes, R. Butler and D.P. Almond, Fatigue of metal-composite joints with penetrative reinforcement, *Proceedings of the 54th AIAA/ASME/ASCE/ASC structures, structural dynamics and materials conference, Boston, USA, April 8-11, 2013*, pp. 6400-6409 (doi: 10.2514/6.2013-1879).